

22 GHz Water Maser Search in 37 Nearby Galaxies

Four New Water Megamasers in Seyfert 2 and OH Maser/Absorber Galaxies

J. Wagner

Max Planck Institute for Radio Astronomy, Auf dem Hügel 69, Bonn, 53121 Germany
e-mail: jwagner@mpi.fr.de

Received September 12, 2013 / Accepted October 21, 2013

ABSTRACT

Aims. We report four new 22 GHz H₂O water masers found in a Green Bank Telescope search toward 37 nearby objects. Our goal was to find new maser galaxies, AGN disk-masers, and objects where both hydroxyl and water maser species coexist.

Methods. We observed 37 sources within 250 Mpc that were selected by high X-ray luminosity ($L_X > 10^{40}$ W) and high absorbing column density ($N_H \gtrsim 10^{22}$ cm⁻²). Sources included dual or triple AGN and interacting systems. We also searched objects detected in hydroxyl (OH). A catalog of 4038 known H₂O (non-)detections was assembled to avoid unnecessary reobservations. The final selection consisted of 16 new sources, 13 non-detections to follow up with a factor ten higher sensitivity, 10 OH masers and one deep OH absorber, of which 37 were observed.

Results. Water megamasers were detected towards the Sy 2 galaxy 2MFGC 13581, towards the 6 GHz OH absorber NGC 4261, and towards the two 1.6 GHz OH maser sources IRAS 17526+3253 and IRAS 20550+1656. We set upper limits on 33 non-detections. The detection rate was 25 % in OH galaxies and 11 % overall. The mean sensitivity was 4 mJy over 24.4 kHz (0.31 km s⁻¹), or between 0.1 L_\odot and 1.0 L_\odot rms for the distances covered by the source sample. Combined with other searches, a total of 95 objects have now been searched for both OH and H₂O masers.

Conclusions. The maser features in 2MFGC 13581 are typical of a sub-parsec accretion disk whereas NGC 4261 likely has jet-masers in a masing torus. The NGC 4261 galaxy (3C 270; dusty torus, twin-jet) and its masers appear similar to NGC 1052 where continuum seed emission by a twin-jet supports masers in the torus. VLBI imaging is required to determine the masing regions in NGC 4261 and 2MFGC 13581. IRAS 17526+3253 has narrow 350 L_\odot systemic masers and the tentative 5 σ detection in IRAS 20550+1656 (II Zw 96) strongly resembles massive star formation kilomasers in NGC 2146. The latter two detections increase the number of known "dual-species" objects containing both OH and H₂O masers to eight. Further we found the overall dual-species detection rate (8 in 95) to be of the order of the joint probability of both species independently occurring in the same object (1 % lower bound). However, this needs to be verified by a more detailed analysis that accounts for the individual selection criteria of the 95 searched objects. Lastly, we see a lack of H₂O kilomasers in OH megamaser objects already noted by Tarchi et al. (2011). This may be due to sensitivity bias rather than astrophysical reasons.

Key words. Masers – Surveys

1. Introduction

Water masers (H₂O; 22.23508 GHz, $6_{16} \rightarrow 5_{23}$) and hydroxyl masers (OH; 1665 MHz and 1667 MHz) in the megamaser class have luminosities that far exceed their Galactic counterparts. They are best known as probes into some extreme environments such as merging galaxies, nuclear starbursts in molecular tori at 100 pc scales in the case of OH, and AGN accretion disks at sub-pc scales, outflows, and the vicinity of jets in the case of H₂O. Water disk-masers are of particular interest and are found between an outer circumnuclear region of molecular gas that is too cold for maser excitation, and an inner atomic gas region that is too hot (> 8000 K) for the molecular gas phase. The kinematics and VLBI angular positions of disk- or torus-masers allow a well-constrained estimate of the central binding mass as in Mrk 273 (Klöckner & Baan 2004), with more accurate mass estimates made with H₂O megamaser observations (Kuo et al. 2011). Additionally, H₂O disk-masers like in UGC 3789 allow a direct measurement of angular diameter distance and the Hubble constant (Reid et al. 2013).

To date, over 4030 galaxies have been searched for H₂O masers, resulting in about 150 detections that include about 20 disk-maser galaxies (see e.g., Nakai et al. 1995; Braatz et al. 1997; Henkel et al. 2005; Kondratko et al. 2006; Braatz & Gugliucci 2008; Bennert et al. 2009; and the project web sites Water Maser Cosmology Project (WMCP)¹ and Megamaser Cosmology Project (MCP)²). In comparison, about 500 galaxies have been searched for OH masers, 120 were detected (at up to $z = 0.265$), and about 10 exhibit OH in absorption (see e.g. Klöckner 2004; Impellizzeri 2008).

Sources that maser in both molecules are extremely rare. This may be expected, since extragalactic OH and H₂O maser species have a quite different pumping mechanism. While OH is radiatively pumped in regions of enhanced density by AGN or star formation photons reprocessed via ≥ 45 K dust to 35/53 μ m infrared (IR), gas phase H₂O is collisionally pumped at ≥ 400 K.

Nevertheless, five objects that maser in both species are known: OH and H₂O kilomasers (OH KM, H₂O KM;

¹<https://www.cfa.harvard.edu/~lincoln/demo/HoME/>

²<https://safe.nrao.edu/wiki/bin/view/Main/MegamaserCosmologyProject>

$L_{\text{OH}}, L_{\text{H}_2\text{O}} < 10 L_{\odot}$) coexist in the starbursts NGC 253 (Frayser et al. 1998; Henkel et al. 2004) and M 82 (Baudry & Brouillet 1996; Argo et al. 2007), an OH KM and an H₂O megamaser (OH MM, H₂O MM; $L_{\text{OH}}, L_{\text{H}_2\text{O}} > 10 L_{\odot}$) are found in the Sy 2 NGC 1068 (Gallimore et al. 1996) and radio-quiet Sy 2 AGN NGC 3079 (Baan & Irwin 1995), whereas Arp 299 is the only OH MM and H₂O MM object (Tarchi et al. 2007). No source with an OH MM and an H₂O KM has yet been found, likely because H₂O KM tend to occur in nearby objects, whereas OH MM are found up to high redshifts where H₂O KM emission falls below sensitivity limits (see Tarchi et al. 2011).

There is no clear general link between OH and H₂O maser species in such "dual-species" objects. However, OH maser emission (and OH seen in absorption) may point towards sources that contain denser molecular regions and a generally larger reservoir of H₂O; OH is formed from the evaporation and dissociation of grain-bound H₂O (Lo 2005; Hollenbach et al. 2009). A larger H₂O abundance may favor a H₂O maser detection. Furthermore, both H₂O KM, OH KM and OH MM have a similar association with, amongst others, star forming regions and nuclear regions with bursts of intense star formation (Lo 2005). We consider that in a H₂O maser search, earlier OH detections could be one of the selection criteria that might increase the detection rate.

The search presented here attempts to identify new water maser galaxies, new dual maser species objects and in particular any H₂O KM in an OH MM galaxy, as well as new AGN disk-maser galaxies suitable for constraining the Hubble constant.

2. Source sample

We considered only sources within 250 Mpc ($< 16\,000 \text{ km s}^{-1}$). We first assembled a database of initially over 8000 known water maser detections and non-detections published in the literature, including WMCP and MCP project web site catalogs of published and unpublished maser search results. We then used an automated NASA/IPAC Extragalactic Database (NED) lookup of source coordinates and name aliases to merge duplicates. This produced a final catalog of 4038 unique objects already observed for H₂O.

Next we identified 126 galaxies in the catalog with a low sensitivity H₂O non-detection (40 mJy to 200 mJy rms) that could be reobserved with a factor 10 higher sensitivity. To identify new sources not yet observed at 22 GHz, we reviewed recent X-ray and AGN data and literature, including recent extragalactic hydroxyl searches (e.g. Klöckner 2004; Impellizzeri 2008). We chose objects with 2–10 keV X-ray data, high X-ray luminosities ($L_X > 10^{40} \text{ W}$) and large absorbing column densities ($N_{\text{H}} \gtrsim 10^{22} \text{ cm}^{-2}$) as found in over 90% of water maser galaxies (e.g. Kondratko et al. 2006; Zhang et al. 2006; Greenhill et al. 2008), and that have a nucleus classified as NLS1, Sy 1.5 to Sy 2.0, LINER or HII region. Some of the sources are also Infrared Astronomical Satellite (IRAS) survey objects with OH masers or OH seen in absorption.

The final selection of 40 nearby galaxies, mergers, binary AGN and triple AGN systems is shown in Table 2 and consists of 17 previous non-detections at $\geq 40 \text{ mJy rms}$, 10 objects with OH seen in emission at 1.6 GHz (3 being previous H₂O non-detections), 1 source with strong OH absorption at 6 GHz (a previous H₂O non-detection), and 16 other sources not yet observed for 22 GHz water masers. Out of this sample, OH maser galaxy ESO 320-G030 had the highest IRAS 100 μm flux density (46 Jy).

Table 1. Observation dates.

Epoch	Start time (UT)	Hours	τ_0
1	2013-02-21 20:30	3:15	0.036–0.037
2	2013-03-02 03:45	3:45	0.047
	2013-03-02 07:30	1:30	0.043
	2013-03-02 09:00	1:30	0.041
3	2013-03-03 18:30	2:15	0.036
	2013-03-03 20:45	1:15	0.033
4	2013-03-09 11:15	2:15	0.036–0.035

Notes. Start time, duration in hours and τ_0 zenith opacity at 21 GHz of the four K-band observing runs in project GBT13A-172.

3. Observations

To uncover kilomasers among the source sample a 4 mJy rms target sensitivity over 24.4 kHz (about 0.31 km s^{-1}) was chosen, equivalent to between $0.1 L_{\odot}$ rms and $1.0 L_{\odot}$ rms in isotropic luminosity. Observations were carried out in four runs during February and March 2013 under project AGBT13A-172 using the National Radio Astronomy Observatory (NRAO³) Robert C. Byrd Green Bank Telescope (GBT). Sessions were scheduled in late winter under good 22 GHz weather conditions. UTC date and time and zenith opacity τ_0 are listed in Table 1. Excellent weather conditions (zenith $\tau_0 = 0.033$ to 0.047) and low T_{sys} (35 K to 75 K) allowed most of the 40 sources to be observed in 16 hours, spending between 12 and 20 minutes on each source and the remainder on calibration.

We used the GBT Spectrometer backend and GBT K-band Focal Plane Array (KFPA) receiver, and selected two KFPA elements near the cryo cooler with the lowest T_{rx} ($< 25 \text{ K}$ over 75% of the band). Beams were 33'' FWHM with an aperture efficiency η_{ap} of 0.66 at 21 GHz and had a 94.9'' beam separation. Observations were in dual-circular polarization and had a 30 second dual-beam "nod" cycle. Both 200 MHz frequency windows of each polarization (i.e. 4 windows in total) were centered on the systemic velocity. The 8192 spectrometer channels were 24.4 kHz wide and covered $V_{\text{sys}} \pm 1250 \text{ km s}^{-1}$.

Pointing and focusing was corrected using strong standard calibrators ($> 0.8 \text{ Jy}$). GBT dynamic corrections compensated for gravitational and thermal surface deformations and remained stable. The full setup was occasionally verified using brief pointings at megamaser galaxies NGC 1068, NGC 3079 and NGC 5793. Pointing and focusing were repeated every 1.5 to 2 hours and after sunrise, with only small adjustments ($< 2.5''$ and $< 8 \text{ mm}$). Wind speeds were low with little to no cloud cover. Zenith opacity measurements τ_0 at 21 GHz were supplied by nearby weather stations and remained stable during the observing runs.

4. Data reduction

A conservative estimated of the flux scale accuracy is $\leq 15\%$. All sources were observed in total power mode with T_{cal} noise injection to determine T_{sys} . Although T_{cal} has a nominal accuracy of 1%, slow temporal drifts degrade it to 10% – 15% typical. The initial aperture efficiency $\eta_{\text{ap}0}$ calculated by the GBTIDL toolbox was corrected for elevation via the

³The National Radio Astronomy Observatory is a facility of the National Science Foundation operated under cooperative agreement by Associated Universities, Inc.

GBT 22.236 GHz gain-elevation curve⁴ of April 8, 2008 that is based on the current Zernike model (*FEM plus 2005WinterV2*) for the GBT adaptive surface. The correction curve is $\eta_{ap} = \eta_{ap0} * (0.910 + 0.00434 * ZD - 5.22 \times 10^{-5} * ZD * ZD)$ where $ZD = 90^\circ - \text{elevation}$ is the angle off zenith.

Nod scans were processed in GBTIDL. The τ_0 and η_{ap} gain corrections were applied first. Next, subspectra affected by internal RFI or spectrometer faults were flagged. To improve the SNR, the blank sky reference subspectra (for subtracting the standing wave across the band) were smoothed with a short 4 to 32 channel boxcar function. Care was taken to avoid introducing artifacts. Third order baselines were removed from individual subspectra. All subspectra and both polarizations were time averaged into a Stokes I spectrum and a final 3rd-order baseline fit was removed. Sensitivity was calculated over line-free channels without smoothing.

For each detection, Gaussian models $S(\nu) = a * e^{-(\nu-\mu)^2/2\sigma_\nu^2}$ were fitted into the calibrated non-smoothed spectra to estimate line peak a (Jy), center μ (km s⁻¹) and FWHM width w (km s⁻¹). The integrated line profile $S_{\text{int}} = \int_{-\infty}^{+\infty} S(\nu) d\nu$ (Jy km s⁻¹) for a single Gaussian $S(\nu)$ equals $a \sigma_\nu \sqrt{2\pi}$. Further noting that $\sigma_\nu = w/2.35482$, and using the luminosity distance D_L and redshift z of the source, the equivalent isotropic luminosity of

$$\frac{L_{\text{iso}}}{L_\odot} = 0.023 \times \frac{S_{\text{int}}}{[\text{Jy km s}^{-1}]} \times \frac{1}{1+z} \times \left(\frac{D_L}{[\text{Mpc}]} \right)^2 \quad (1)$$

can be written for the fitted Gaussians in form of the sum

$$\frac{L_{\text{iso}}}{L_\odot} = \frac{0.023 \sqrt{2\pi}}{2.35482} \times \frac{\sum_i a_i \cdot w_i}{[\text{Jy km s}^{-1}]} \times \frac{1}{1+z} \times \left(\frac{D_L}{[\text{Mpc}]} \right)^2 \quad (2)$$

over all Gaussian components (see also Bennert et al. 2009). The factor 0.023 contains unit conversions and the water maser rest frequency (for 1.6 GHz OH masers the factor is 0.0017). Upper luminosity limits for water maser non-detections are given for single wide Gaussian H₂O line with 2.0 km s⁻¹ FWHM and a 3 σ peak. The luminosities for detections are based on Eq. 1, with S_{int} evaluated directly over the line regions of the spectrum using Simpson's Rule. Spectra of the detections presented here were smoothed with a 3rd order 9-point (2.79 km s⁻¹) Savitzky-Golay shape-preserving filter to reduce the noise floor by 70% while maintaining the shape and height of the maser features.

5. Results and Discussion

Of the 40 sources listed in Table 2, 37 were observed for H₂O masers with a detection rate of 11%. Three sources have a strong maser detection and one has a tentative detection. The spectra are shown in Figure 1. Interestingly, three detections are in the set of 11 sources that are also detected in hydroxyl in emission or in deep absorption. No spectra were captured for three sources (NGC 3341, NGC 7130 and ESO 323-G077). The observed sources, sensitivities and isotropic luminosities (H₂O and OH), and absorbing column densities are given in Table 2. The luminosity distances, source redshifts and recession velocities, v_{LSR} , were adopted from NED. Recession velocities use the optical definition and are in the kinematic Local Standard of Rest (LSR).

Selection by X-ray data did not appear to enhance the H₂O maser detection rate. In our sample, 14 active galaxies have

⁴<https://safe.nrao.edu/wiki/bin/view/GB/Observing/GainPerformance>

a published X-ray absorbing column density. Two of these yielded a H₂O MM detection. One source hosts a heavily obscured AGN ($N_{\text{H}} > 10^{23}$ cm⁻²) and the other a Compton-thick AGN ($N_{\text{H}} \geq 10^{24}$ cm⁻²). This is consistent with Castangia et al. (2013) who find 96% (45/47) of H₂O MM sources have $N_{\text{H}} > 10^{23}$ cm⁻². However, the same two sources were also selected by OH, resulting in a better detection rate given by the OH selection (3/11) rather than the X-ray selection (2/14).

Below we discuss the four water maser detections.

5.1. 2MFGC 13581

A new H₂O disk-MM is found in the optically edge-on galaxy 2MFGC 13581 ($v_{\text{LSR}} = 10309 \pm 42$ km s⁻¹ (Hopp et al. 2000), $D_L = 145$ Mpc, $z = 0.034$). It is the second-closest of six Seyfert candidates in the Hamburg/SAO survey for emission-line galaxies and is a probable Sy 2 (Hopp et al. 2000). Masers are detected in two high-velocity groups, symmetrically offset from the systemic velocity by about ± 390 km s⁻¹. No systemic emission is detected and has a 3 σ upper limit of 6.3 mJy. The red group peaks at 25 mJy and forms a forest of ≈ 3 km s⁻¹ FWHM lines, similar to the blue group that peaks at 20 mJy. Each group can be approximated by a wide profile, with the blue one centered at 9940 km s⁻¹ (5.3 mJy peak, 61.5 km s⁻¹ FWHM) and the red one at 10724 km s⁻¹ (4.4 mJy peak, 114.4 km s⁻¹ FWHM). Their mean, 10332 km s⁻¹, lies within 1 σ of the systemic recession velocity. The blue and red groups have luminosities of 120 L_\odot and 170 L_\odot , respectively.

The symmetric spectrum suggests that emission most likely originates from a circumnuclear masing disk. The absence of systemic emission may be explained by a warp in the disk that shadows parts of the disk from the X-ray emission by the central engine that is thought to support maser emission (Neufeld et al. 1994). The undetected systemic masers may also have a quite low flux density. Alternatively, they may be highly variable like the systemic (disk-)maser emission in Circinus and thus not always detected (Greenhill et al. 2003; McCallum et al. 2009).

We can estimate the radius of the masing disk annulus in 2MFGC 1358 if we assume Keplerian rotation, a black hole mass of $10^7 M_\odot$ typical of other disk-maser galaxies (e.g. Kuo et al. 2011), and a fully edge-on disk. The observed orbital velocity of ± 390 km s⁻¹ then translates into a 0.4 parsec (0.8 mas) average disk diameter. Unfortunately, given the low maser flux, prospects for a successful VLBI map and a determination of variability and the secular acceleration of possibly existing weak systemic maser components are poor.

5.2. IRAS 17526+3253

Water megamasers in this IR galaxy (UGC 11035; $v_{\text{LSR}} = 7818 \pm 9$ km s⁻¹ (de Vaucouleurs et al. 1991), $D_L = 108$ Mpc, $z = 0.026$ (NED), $L_{\text{IR}} \approx 7 \times 10^{11} L_\odot$ estimated from IRAS fluxes using the method by Wouterloot & Walmsley 1986) have a relatively high peak flux of ≈ 170 mJy. Emission appears in a narrow, slightly blueshifted 40 km s⁻¹ window around the systemic velocity. It has three features: two wider profiles at 7797 km s⁻¹ (47 mJy peak, 4.0 km s⁻¹ FWHM, 50 L_\odot) and 7810 km s⁻¹ (65 mJy peak, 10.9 km s⁻¹ FWHM, 210 L_\odot), and a narrow emission line at 7808 km s⁻¹ (170 mJy peak, 2.2 km s⁻¹ FWHM, 100 L_\odot).

Literature lists UGC 11035 as an OH KM galaxy. An early non-detection ($L_{\text{OH}} < 4 L_\odot$ at 1.0 mJy rms) by Garwood et al. (1987) was followed by a broad blueshifted feature (3.7 mJy

peak, $L_{OH} = 6.46 L_{\odot}$) detected near 7450 km s^{-1} by Martin et al. 1989 but no spectrum was published. A recent observation suffered from RFI and had insufficient sensitivity to confirm the kilomaser (McBride & Heiles 2013).

The 2MASS image shows two near-infrared components separated by $60''$ (about 30 kpc) with an angular size ratio of ≈ 5 . The image suggests UGC 11035 could be a major merger system. The hard X-ray luminosity would then be expected to exceed $10^{43} \text{ erg s}^{-1}$. This would contribute to enhanced IR luminosity through core emission reprocessed in the dense concentration of gas accumulated during the merger event. Using $60 \mu\text{m}$, $100 \mu\text{m}$ and $S_{1.4\text{GHz}}$ flux points from NED, the q parameter (see e.g. Yun et al. 2001) of this galaxy is 4.74, indicating an IR excess. The q is notably higher than 2.34 ± 0.01 of the IRAS 2 Jy sample (Yun et al. 2001) and exceeds 2.57 ± 0.36 of typical OH MM galaxies (Klöckner 2004), indicating a buried AGN or enhanced star formation. UGC 11035 also has a curiously flat velocity field of 210 km s^{-1} at 9 kpc from the center, suggesting either a giant irregular galaxy or interaction of two face-on objects. The inner 18 kpc have a kinematic mass of $\approx 10^{11} M_{\odot}$ (Andreasian 1992; Andreasian & Alloin 1994).

Given limited data on the object we speculate that H_2O emission might originate from a small shocked region in an ongoing merger similar to Arp 299. The maser features lack the high velocities associated with jet and nuclear outflow masers (e.g. Greenhill et al. 2003). Their velocity span of 40 km s^{-1} is narrow, but still typical of star formation masers. Assuming a buried AGN gives rise to the IR excess, the systemic masers may also be associated with a slightly inclined, not fully edge-on warped accretion disk. A warp along the line of sight towards the nucleus can compensate for the disk inclination and produce the velocity coherent path lengths necessary for luminous systemic maser emission. Monitoring for secular line accelerations or a VLBI observation are required to rule out a nuclear association.

5.3. NGC 4261

The WMAP project lists the giant elliptical galaxy NGC 4261 ($v_{\text{LSR}} = 2240 \pm 7 \text{ km s}^{-1}$ (Trager et al. 2000), $D_L = 35.6 \text{ Mpc}$, $z = 0.0075$) as a 109 mJy rms non-detection observed in 2002. We reached 3.1 mJy rms and detect broad emission that is fitted by a single Gaussian of 10.3 mJy, 154 km s^{-1} FWHM centered on 2302 km s^{-1} . Peak emission is redshifted by about $+60 \text{ km s}^{-1}$ relative to the systemic velocity and has a total isotropic luminosity of $50 L_{\odot}$.

NGC 4261 is a LINER galaxy associated with the low-luminosity FR-I radio source 3C 270 that launches a highly symmetric kpc-scale twin jet. The galaxy is known for its 240 pc nuclear torus/disk found by the Hubble Space Telescope. The nucleus hosts a $4.9 \times 10^8 M_{\odot}$ SMBH and has an X-ray absorbing column density N_{H} of $> 5 \times 10^{22} \text{ cm}^{-2}$ (Gliozzi et al. 2003). Recent hard X-ray data show a slightly higher obscuring column density of $16.4_{13.25}^{21.64} \times 10^{22} \text{ cm}^{-2}$ (González-Martín et al. 2009a).

VLBI shows neutral HI absorption against the counter-jet, with deepest absorption at 2260 km s^{-1} , redwards with respect to the systemic velocity. It has been modeled by atomic gas in a thin disk with an absorbing column density of $N_{\text{H}} \approx 10^{21} \text{ cm}^{-2}$ (van Langevelde et al. 2000). There is also deep OH absorption at 6 GHz against a 1.3 Jy continuum with a 400 km s^{-1} FWHM around the systemic velocity (Impellizzeri 2008).

With the presence of a low-luminosity core, an optical dusty torus, molecular absorption and a twin radio jet, NGC 4261 is remarkably similar to the twin-jet LINER NGC 1052. The spectrum of NGC 1052 has a single, broad and slightly red-

shifted luminous 150 mJy maser feature. VLBI observations of NGC 1052 found water masers in two regions along the jet axis. Emission has been associated with continuum seed emission from jet blobs being amplified in a X-ray dissociation region located on the inner surface of a torus at a typical (for a J-type shock) temperature of 400 K (Sawada-Satoh et al. 2008). Given the evidence for abundant HI and OH molecules and a high X-ray absorbing N_{H} column density towards NGC 4261, combined with the radio jet and the maser profile, a masing torus region with gas infalling at $+60 \text{ km s}^{-1}$ seems plausible. Existing VLBI datasets map only NGC 4261 continuum emission and do not cover the maser frequency range. A VLBI follow-up is required to determine a masing torus association.

5.4. IRAS 20550+1656

We tentatively find broad megamasers in the LIRG/ULIRG irregular galaxy IRAS 20550+1656 (II Zw 96; $v_{\text{LSR}} = 10837 \pm 10 \text{ km s}^{-1}$ (Giovannelli & Haynes 1993), $D_L = 148 \text{ Mpc}$, $z = 0.036$). With Arp 299, IRAS 20550+1656 may be the second galaxy that hosts megamasers of both the OH and H_2O species. The sensitivity was 5.8 mJy per 0.3 km s^{-1} channel and 1.5 mJy after 16-channel Gaussian smoothing. Two 9 mJy features are seen at $\pm 110 \text{ km s}^{-1}$ around the recessional velocity. The combined isotropic luminosity of the blue 10737 km s^{-1} feature (9.0 mJy peak, 102.8 km s^{-1} FWHM) and the red 10957 km s^{-1} feature (9.1 mJy peak, 96.4 km s^{-1} FWHM) is relatively high with $600 L_{\odot}$. Narrower features seem to be symmetrically distributed around the systemic velocity, such as two offset by -380 km s^{-1} and $+420 \text{ km s}^{-1}$, but could also be explained as particularly pronounced baseline ripple. These and the broad features are however persistent over different smoothing settings for the "nod" reference spectra, and different baseline fits prior to averaging all subspectra. The broad masers have a post-fit confidence of somewhat better than 5σ . The GBT integration time was 12 minutes and additional time would be needed for a more robust detection especially of the narrower features.

The object is an ongoing merger or close binary system with a peculiar rotation curve that is known to host an OH MM with 26 mJy peak and $83.2 L_{\odot}$ luminosity (Andreasian 1992; Klöckner 2004). HI is seen in emission with a FWHM of about 200 km s^{-1} (van Driel et al. 2001). XMM-Newton observations found a single X-ray source and a high abundance of alpha process elements suggestive of starburst activity, but could not rule out an AGN or AGN-starburst composite. The X-ray core is either very faint or has an $N_{\text{H}} > 10^{24} \text{ cm}^{-2}$ (Inami et al. 2010; Mudd et al. 2012). Starburst activity would be consistent with earlier optical and IR spectroscopy (Goldader et al. 1997). VLBI observations of the OH MM emission have placed it off-center in a merging system. The OH masers trace a 300 pc region around the second nucleus with a mass of $10^9 M_{\odot}$ that has some probability of being a heavily obscured AGN (Migenes et al. 2011). Spitzer observations found starburst activity similar to extranuclear starbursts in NGC 4038/9 and Arp 299. In the latter, three maser regions are associated with both nuclear regions of Arp 299 and an overlap region (Tarchi et al. 2011). The spectrum of the IRAS 20550+1656 water masers is also strongly reminiscent of that of NGC 2146 with its massive star formation kilomasers. The data are quite suggestive that IRAS 20550+1656 masers can be related to starburst and star formation activity. The maser flux is unfortunately rather low for a VLBI follow-up.

6. Dual maser species

In literature, there are five known sources (or six, if including uncertain OH masers in UGC 5101) that are known to host both OH and H₂O maser species. These "dual-species" objects typically have a complex morphology and the masers are located in unrelated regions. Our two detections in 10 searched OH maser objects increase the number of known dual-species objects to eight.

Tarchi et al. (2011) report 57 sources searched for both 1.6 GHz OH and 22 GHz H₂O maser species. Six are detected in neither species, 45 in only one, and six in both species. Tarchi et al. also note a curious lack of H₂O kilomasers in OH megamaser objects. Adding our sources, and sources common to the 4038-entry H₂O database and recent OH searches (Staveley-Smith et al. 1992; Klöckner 2004; Impellizzeri 2008; Willett et al. 2011), we find a total of 95 sources searched for both transitions, 34 detected in neither, 35 detected in H₂O only, 18 in OH only, and about 8 detected in both species (if the two uncertain OH masers in UGC 5101 and IRAS 17526+3253 are included), for a total of 61 sources detected in at least one of the two maser species. Luminosities, 3σ limits and redshifts of these 61 detected sources are presented in Figure 2. Luminosities against source redshifts for all 95 sources are shown in the inset. The upper limits of the non-detections have a median of $0.04 L_{\odot}$ for OH and $0.4 L_{\odot}$ for H₂O. This demonstrates a large fraction of H₂O kilomasers ($L < 10 L_{\odot}$) may go undetected. The difference in the two medians is partly due to the frequency proportionality of the isotropic luminosity in Eq. 1 – an at least factor 13 higher sensitivity (lower mJy rms) is required for detecting H₂O kilomasers at 22 GHz in a 1.6 GHz OH MM object. The probability of detecting a H₂O KM in OH MM objects is further reduced by the higher average redshift of OH MM galaxies, with currently known H₂O KM galaxies found at redshifts up to 0.014 and OH MM galaxies at redshifts between 0.010 and 0.264.

The six reliable dual-species detections correspond to a conditional water maser detection rate of $P(\text{H}_2\text{O}|\text{OH}) = 25\%$ in the 24 OH galaxies, and a detection rate of $P(\text{OH} \cap \text{H}_2\text{O}|s_1) = 6\%$ for all $N = 95$ targets selected for an OH search by some criteria s_1 such as high infrared flux density. Over current searches, the average detection rate for OH is about $P(\text{OH}|s_1) = 25\%$ (120 in 500) and about $P(\text{H}_2\text{O}|s_2) = 4\%$ for H₂O (150 in 4030), where the selection criteria s_2 typically include starburst or AGN activity, X-ray luminosity or a high absorbing column density N_{H} . Accounting for apparently mutually exclusive pumping mechanisms of the OH and H₂O species and assuming selections s_1 and s_2 are independent (although Tarchi et al. 2004 find a significantly increased H₂O maser detection rate in FIR-luminous sources), the lower bound for the expected probability of two species independently coinciding would be $P(\text{OH} \cap \text{H}_2\text{O}|s_1, s_2) \geq 1\%$, which is on the order of 6% of the $N = 95$ dataset. An accurate estimate of the coincidence rate would require a comparison of the selection criteria of each of the 95 sources, a task that is beyond the current scope.

7. Conclusions and Summary

We detected water megamasers in four galaxies: three in OH galaxies, and one in a Sy 2 galaxy with no previous OH search. The OH MM galaxy IRAS 20550+1656 has a tentative starburst-like H₂O MM detection, the presumed OH KM galaxy IRAS 17526+3253 has narrow 0.17 Jy systemic masers, and the 6 GHz OH absorber NGC 4261 (3C 270) with a twin jet hosts a likely jet-maser. Disk-masers were found towards the

probable Sy 2 AGN in 2MFGC 13581. The black hole mass is unknown, but assuming a mass of $10^7 M_{\odot}$ typical of AGN disk-maser galaxies, the masing disk may be around 0.4 pc in diameter. Masers in NGC 4261 are particularly interesting as the host galaxy and the maser profile are remarkably similar to H₂O MM galaxy NGC 1052. A VLBI map of NGC 4261 may be able to locate regions of a molecular torus excited by a background jet continuum like in NGC 1052. VLBI imaging of disk-maser galaxy 2MFGC 13581 might produce a precise M_{BH} estimate, although the maser flux densities are very low for VLBI. Lack of systemic features in 2MFGC 13581 makes this source less interesting for measuring the angular diameter distance and the Hubble constant. We plan VLBI follow-ups on the more luminous detections in IRAS 17526+3253 and NGC 4261.

Our detection of water masers in two OH maser galaxies updates the current count of six dual-species objects to eight. The conditional H₂O detection rate in OH maser galaxies $P(\text{H}_2\text{O}|\text{OH}) = 25\%$ is higher than the average 4% rate achieved in H₂O maser searches. We could speculate that OH masers point towards systems with an overall larger molecular reservoir or a larger number of over-densities and shocked regions with favorable conditions for producing detectable luminous H₂O maser emission. The dual-species detections in a sample of 95 objects may be explained by a random coincidence of two regions with suitable maser conditions in a single system. However, a more detailed analysis that inspects actual source selection criteria of each of the 95 sources is necessary to determine if dual-species detections are indeed a random coincidence, and if the seemingly enhanced detection rate of H₂O masers in extragalactic objects selected by the presence of OH masers is only a product of the small dataset.

Acknowledgements. I thank Jim Braatz, Christian Henkel, and Alan Roy for introduction to the GBT, discussion during the proposal, and comments on the manuscript. The author was supported for this research through the International Max Planck Research School (IMPRS) for Astronomy and Astrophysics. This research has made use of the NASA/IPAC Extragalactic Database (NED) which is operated by the Jet Propulsion Laboratory, California Institute of Technology, under contract with the National Aeronautics and Space Administration.

References

- Andreasian, N. & Alloin, D. 1994, *A&AS*, 107, 23
- Andreasian, N. K. 1992, in *American Institute of Physics Conference Series*, Vol. 254, American Institute of Physics Conference Series, ed. S. S. Holt, S. G. Neff, & C. M. Urry, 617–620
- Argo, M. K., Pedlar, A., Beswick, R. J., & Muxlow, T. W. B. 2007, *MNRAS*, 380, 596
- Baan, W. A. & Irwin, J. A. 1995, *ApJ*, 446, 602
- Baudry, A. & Brouillet, N. 1996, *A&A*, 316, 188
- Bennert, N., Barvainis, R., Henkel, C., & Antonucci, R. 2009, *ApJ*, 695, 276
- Braatz, J. A. & Gugliucci, N. E. 2008, *ApJ*, 678, 96
- Braatz, J. A., Wilson, A. S., & Henkel, C. 1997, *ApJS*, 110, 321
- Castangia, P., Panessa, F., Henkel, C., Kadler, M., & Tarchi, A. 2013, *ArXiv e-prints*
- de Vaucouleurs, G., de Vaucouleurs, A., Corwin, Jr., H. G., et al. 1991, *Third Reference Catalogue of Bright Galaxies*. Volume I: Explanations and references. Volume II: Data for galaxies between 0^h and 12^h . Volume III: Data for galaxies between 12^h and 24^h .
- Frayer, D. T., Seaquist, E. R., & Frail, D. A. 1998, *AJ*, 115, 559
- Gallimore, J. F., Baum, S. A., O’Dea, C. P., Brinks, E., & Pedlar, A. 1996, *ApJ*, 462, 740
- Garwood, R. W., Dickey, J. M., & Helou, G. 1987, *ApJ*, 322, 88
- Giovanelli, R. & Haynes, M. P. 1993, *AJ*, 105, 1271
- Giozzi, M., Sambruna, R. M., & Brandt, W. N. 2003, *A&A*, 408, 949
- Goldader, J. D., Goldader, D. L., Joseph, R. D., Doyon, R., & Sanders, D. B. 1997, *AJ*, 113, 1569
- González-Martín, O., Masegosa, J., Márquez, I., & Guainazzi, M. 2009a, *ApJ*, 704, 1570

González-Martín, O., Masegosa, J., Márquez, I., & Guainazzi, M. 2009b, *ApJ*, 704, 1570

Greenhill, L. J., Booth, R. S., Ellingsen, S. P., et al. 2003, *ApJ*, 590, 162

Greenhill, L. J., Tilak, A., & Madejski, G. 2008, *ApJ*, 686, L13

Henkel, C., Braatz, J. A., Tarchi, A., et al. 2005, *Ap&SS*, 295, 107

Henkel, C., Tarchi, A., Menten, K. M., & Peck, A. B. 2004, *A&A*, 414, 117

Hollenbach, D., Kaufman, M. J., Bergin, E. A., & Melnick, G. J. 2009, *ApJ*, 690, 1497

Hopp, U., Engels, D., Green, R. F., et al. 2000, *A&AS*, 142, 417

Impellizzeri, C. 2008, *Molecular absorption in the cores of AGN: On the unified model* (Bonn University Dissertations)

Inami, H., Armus, L., Surace, J. A., et al. 2010, *AJ*, 140, 63

Klößner, H. 2004, *Extragalactic Hydroxyl* (Rijksuniversiteit Groningen)

Klößner, H.-R. & Baan, W. A. 2004, *A&A*, 419, 887

Kondratko, P. T., Greenhill, L. J., & Moran, J. M. 2006, *ApJ*, 652, 136

Kuo, C. Y., Braatz, J. A., Condon, J. J., et al. 2011, *ApJ*, 727, 20

Lo, K. Y. 2005, *Annual Review of Astronomy and Astrophysics*, 43, 625

Martin, J.-M., Bottinelli, L., Gouguenheim, L., Le Squeren, A.-M., & Dennefeld, M. 1989, *Academie des Sciences Paris Comptes Rendus Serie Sciences Mathematiques*, 308, 287

McBride, J. & Heiles, C. 2013, *ApJ*, 763, 8

McCallum, J. N., Ellingsen, S. P., Lovell, J. E. J., Phillips, C. J., & Reynolds, J. E. 2009, *MNRAS*, 392, 1339

Migenes, V., Coziol, R., Cooperider, K., et al. 2011, *MNRAS*, 416, 1267

Mudd, D., Mathur, S., Guainazzi, M., et al. 2012, *ApJ* (submitted)

Nakai, N., Inoue, M., Miyazawa, K., Miyoshi, M., & Hall, P. 1995, *PASJ*, 47, 771

Neufeld, D. A., Maloney, P. R., & Conger, S. 1994, *ApJ*, 436, L127

Noguchi, K., Terashima, Y., & Awaki, H. 2009, *ApJ*, 705, 454

Reid, M. J., Braatz, J. A., Condon, J. J., et al. 2013, *ApJ*, 767, 154

Risaliti, G., Maiolino, R., & Salvati, M. 1999, *ApJ*, 522, 157

Sawada-Satoh, S., Kamenno, S., Nakamura, K., et al. 2008, *ApJ*, 680, 191

Staveley-Smith, L., Norris, R. P., Chapman, J. M., et al. 1992, *MNRAS*, 258, 725

Tan, Y., Wang, J., & Zhang, K. 2012, *Science in China G: Physics and Astronomy*, 55, 2482

Tarchi, A., Castangia, P., Henkel, C., & Menten, K. M. 2007, *New A Rev.*, 51, 67

Tarchi, A., Castangia, P., Henkel, C., Surcis, G., & Menten, K. M. 2011, *A&A*, 525, A91

Tarchi, A., Henkel, C., Peck, A., et al. 2004, in *Astronomical Society of the Pacific Conference Series*, Vol. 320, *The Neutral ISM in Starburst Galaxies*, ed. S. Aalto, S. Huttemeister, & A. Pedlar, 199

Trager, S. C., Faber, S. M., Worthey, G., & González, J. J. 2000, *AJ*, 119, 1645

van Driel, W., Gao, Y., & Monnier-Ragaigne, D. 2001, *A&A*, 368, 64

van Langevelde, H. J., Pihlström, Y. M., Conway, J. E., Jaffe, W., & Schilizzi, R. T. 2000, *A&A*, 354, L45

Vasudevan, R. V., Brandt, W. N., Mushotzky, R. F., et al. 2013, *ApJ*, 763, 111

Willett, K. W., Darling, J., Spoon, H. W. W., Charmandaris, V., & Armus, L. 2011, *ApJ*, 730, 56

Wouterloot, J. G. A. & Walmsley, C. M. 1986, *A&A*, 168, 237

Yun, M. S., Reddy, N. A., & Condon, J. J. 2001, *ApJ*, 554, 803

Zhang, J. S., Henkel, C., Kadler, M., et al. 2006, *A&A*, 450, 933

Table 2. Source sample of the 22 GHz H₂O maser search

Source	Epoch	Position (α_{2000} δ_{2000})	V_{sys} (km s^{-1})	$1\sigma S_{22}$ (mJy)	S_{22} (mJy)	L_{22} (L_{\odot})	$L_{1.6}$ (L_{\odot})	N_{H} (cm^{-2})	Notes
01 IRAS 00160-0719 ^(a)	3	00:18:35.9 -07:02:56.0	5396	2.9	< 8.7	< 2.06			Sy2+HII
02 ESO 350-IG038 ^(a)	3	00:36:52.7 -33:33:17.0	6175	4.6	< 13.8	< 4.48			pair, LIRG, HII/SB
03 IRAS 00494-3056 ^(a)	3	00:51:51.8 -30:40:00.0	15529	5.3	< 15.9	< 34.86			SB, ULIRG
04 NGC 0315 ^(a)	3	00:57:48.9 +30:21:09.0	4942	3.0	< 9.0	< 1.54		5.0×10^{22}	LINER(?), jet
05 NGC 0526A	1	01:23:54.4 -35:03:56.0	5725	4.3	< 12.9	< 3.62		2.0×10^{22}	Sy1.9
06 IRAS 01418+1651	3	01:44:30.5 +17:06:05.0	8225	2.9	< 8.7	< 5.11	245.0		Sy2, LIRG
07 NGC 0833	1	02:09:20.8 -10:08:59.0	3864	2.9	< 8.7	< 1.05		2.7×10^{23}	Sy2/LINER
08 NGC 0925 ^(a)	3	02:27:16.9 +33:34:45.0	553	2.7	< 8.1	< 0.03			LLAGN
09 IC 1858 ^(a)	1	02:49:08.4 -31:17:22.0	6070	3.5	< 10.5	< 3.41			LINER(?)
10 IRAS 02580-1136	1	03:00:30.6 -11:24:57.0	8962	3.5	< 10.5	< 8.37		5.6×10^{23}	Sy2+HII, merger
11 NGC 1167 ^(a)	1	03:01:42.4 +35:12:21.0	4945	2.7	< 8.1	< 1.70		3.0×10^{21}	Sy2/LINER, jet
12 NGC 1275 ^(a,b)	3	03:19:48.1 +41:30:42.0	5264	26.4	< 79.2	< 17.73		1.5×10^{22}	Sy1.5
13 IRAS F04023-1638 ^(a)	1	04:04:40.6 -16:30:14.0	8643	3.1	< 9.3	< 6.37			n/a
14 IRAS 04332+0209	1	04:35:48.4 +02:15:29.0	3590	2.7	< 8.1	< 0.93	1.9		HII
15 MCG+02-21-013	2	08:04:46.4 +10:46:36.0	10323	4.1	< 12.3	< 12.93			pair, Sy2+Sy1
16 NGC 2974	2	09:42:33.3 -03:41:57.0	1919	3.0	< 9.0	< 0.27			Sy2, SF
17 ESO 374-IG032 ^(a)	2	10:06:05.1 -33:53:17.0	10223	5.3	< 15.9	< 16.49	724.0		LIRG, merger, pair
18 NGC 3341	–	10:42:31.5 +05:02:38.0	8196	–	–	–			Sy2+LINER+comp
19 UGC 05881	2	10:46:42.5 +25:55:54.0	6173	2.9	< 8.7	< 3.40		2.5×10^{24}	LINER
20 NGC 3563B ^(a)	2	11:11:25.2 +26:57:48.9	10774	3.0	< 9.0	< 10.35			jet, FSRs
21 NGC 3655 ^(a)	2	11:22:54.6 +16:35:24.1	1473	2.8	< 8.4	< 0.39			HII
22 ESO320-G030 ^(a)	2	11:53:11.7 -39:07:49.0	3232	6.9	< 20.7	< 2.41	33.0		LIRG, SB, AGN
23 NGC 4261 ^(a,c)	2	12:19:23.2 +05:49:31.0	2238	3.1	10.3	50	abs.		LINER, twin-jet
24 NGC 4939 ^(a)	4	13:04:14.4 -10:20:23.0	3110	12.8	< 38.4	< 2.83		$> 1.0 \times 10^{25}$	Sy2
25 ESO 323-G077	–	13:06:26.1 -40:24:53.0	4501	–	–	–		5.5×10^{23}	Sy1.2/LINER
26 UGC 8327	2	13:15:15.6 +44:24:26.0	11002	2.7	< 8.1	< 9.55		5.2×10^{22}	Sy2+Sy2
27 IC 4374 ^(a)	2	14:07:29.8 -27:01:04.3	6535	4.0	< 12.0	< 5.16		$> 8.0 \times 10^{21}$	FSRS, FRII
28 NGC 5806	2	15:00:00.4 +01:53:29.0	1359	3.4	< 10.2	< 0.32			Sy2
29 IRAS 15065-1107 ^(a)	2	15:08:49.1 -11:12:28.0	2105	3.6	< 10.8	< 0.53	1.1		pair
30 IRAS 15179+3956	4	15:19:47.1 +39:45:38.0	14261	2.9	< 8.7	< 16.92	10.5		2core, HII
31 Ark 481 ^(a)	2	15:39:05.2 +05:34:16.6	7781	3.3	< 9.9	< 5.82			n/a
32 IRAS 16399-0937	2	16:42:40.2 -09:43:14.0	8098	3.9	< 11.7	< 7.25	47.0		Sy2+HII/LINER
33 2MFGC13581	2+4	16:58:15.5 +39:23:29.0	10290	2.1	25.5	290			Sy2
34 IRAS 17208-0014	2+4	17:23:21.9 -00:17:01.0	12834	2.5	< 7.5	< 11.54	1090.0	5.2×10^{21}	HII, LINER, SB
35 IRAS 17526+3253	4	17:54:29.4 +32:53:14.0	7798	5.3	170	360	6.5		ULIRG, LINER(?)
36 UGC 11185NED01	2	18:16:09.4 +42:39:23.0	12426	3.0	< 9.0	< 12.81			Sy2+Sy2
37 IRAS 20550+1656	4	20:57:23.9 +17:07:39.0	10822	5.8 ^(d)	9.1	600	83.2	$> 1.0 \times 10^{24}$	LIRG, HII, pair
38 NGC 7130	–	21:48:19.5 -34:57:04.0	4842	–	–	–		$> 6.0 \times 10^{23}$	Sy2/LINER/HII
39 UGC 12237	3	22:54:19.7 +11:46:57.0	8476	3.1	< 9.3	< 7.01		1.9×10^{23}	Sy2/SB, SNIa
40 NGC 7742	3	23:44:15.8 +10:46:01.0	1663	1.8	< 5.4	< 0.13			Sy2/LINER, SB, HII

Notes. Epochs refer to observing dates (see Table 1). The three sources without epochs were not observed. Optical heliocentric recession velocities (V_{sys}) are adopted from NED. The maser search covered $V_{\text{sys}} \pm 1250 \text{ km s}^{-1}$. The flux scale is accurate to better than 15%. Sensitivity ($1\sigma S_{22}$) is the rms over the line-free 75% of the 200 MHz band and is derived from 24.4 kHz channels without smoothing. The peak flux (S_{22}) and total equivalent isotropic luminosity (L_{22}) are stated for detections (sources in bold; 23, 33, 35, 37). For non-detections, 3σ upper limits on S_{22} and L_{22} are given, with L_{22} based on $3 \cdot 1\sigma S_{22}$ and a 2.0 km s^{-1} FWHM Gaussian. Sources with hydroxyl (OH) masers are indicated in italic and the OH maser luminosities ($L_{1.6}$) are adopted from Staveley-Smith et al. (1992); Klöckner (2004); Impellizzeri (2008); Willett et al. (2011). The 2–10 keV X-ray absorbing column densities (N_{H}) are adopted from literature (Risaliti et al. 1999; González-Martín et al. 2009b; Noguchi et al. 2009; Tan et al. 2012; Vasudevan et al. 2013). The last column shows the object classification adopted from NED and literature.

Remarks: (a) Source has a previous published or unpublished H₂O non-detection (20 mJy to 200 mJy rms), with references on the WMCP or MCP project pages. (b) The velocity coverage on NGC 1275 was 3000 to 14000 km s^{-1} (800 MHz) to include the infalling object at +3000 km s^{-1} . (c) NGC 4261 exhibits H I in absorption at 1.4 GHz and OH in deep absorption at 6 GHz, but has not been searched for OH at 1.6 GHz (van Langevelde et al. 2000; Impellizzeri 2008). (d) Sensitivity on IRAS 20550+1656 was 5.8 mJy without smoothing and 1.5 mJy rms after 16-channel Gaussian smoothing.

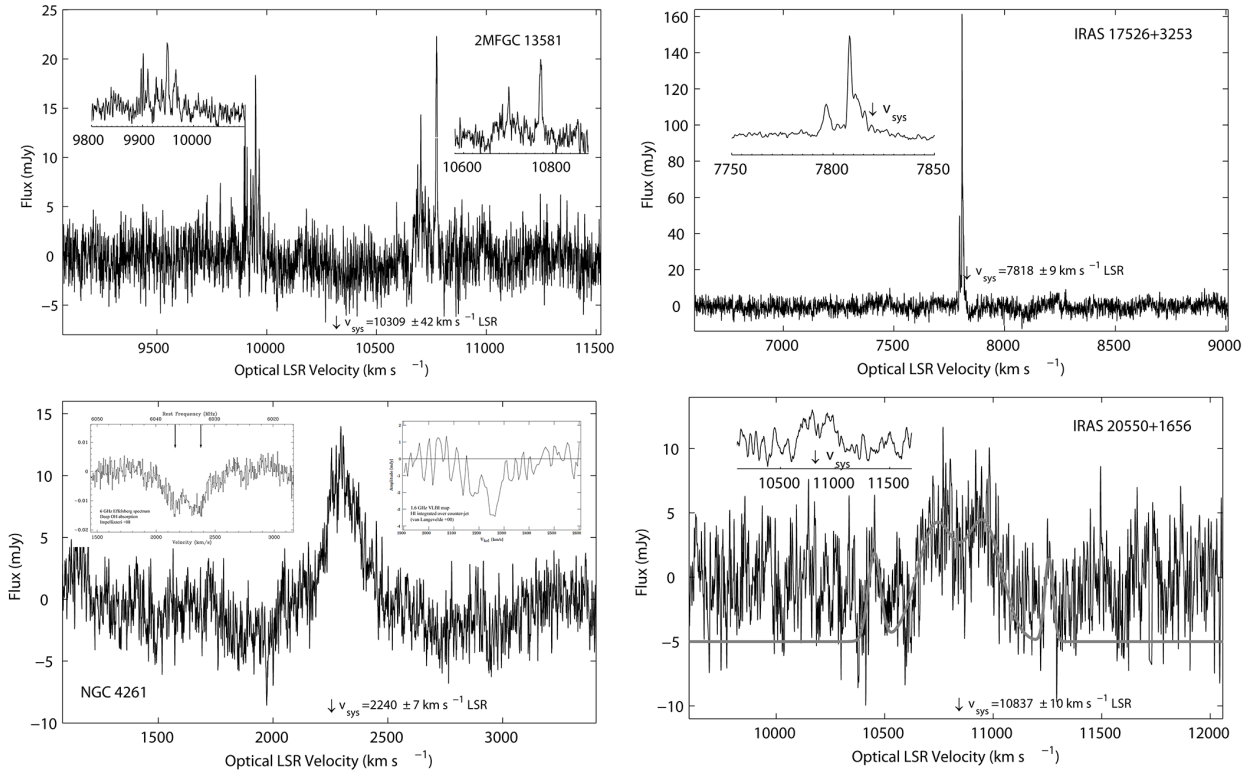


Fig. 1. Spectra of the four 22 GHz water megamasers detections. Velocities are in the kinematic Local Standard of Rest frame (LSR) and use the optical convention. Recession velocities, V_{sys} , are adopted from NED. The channel spacing is 0.3 km s^{-1} . The uncertainty of the flux density scale is $\leq 15\%$. *Top left:* Maser features towards possible Sy 2 galaxy 2MFGC 13581 are typical of masing sub-parsec accretion disks around AGN. *Top right:* IRAS 17526+3253 (UGC 11035) is an OH KM galaxy and has narrow $360 L_{\odot}$ water masers. *Bottom left:* NGC 4261 (3C 270; twin-jet, torus) shows deep H I absorption at 2260 km s^{-1} (right inset) and deep 6 GHz OH absorption at $2100\text{--}2400 \text{ km s}^{-1}$ (left inset) against the counter-jet (insets adopted from van Langevelde et al. 2000; Impellizzeri 2008). The broad H_2O MM feature is slightly redshifted with respect to the systemic velocity. *Bottom right:* IRAS 20550+1656 (II Zw 96) is an OH MM object and has a tentative H_2O MM detection at 5σ after 16-channel Gaussian smoothing (inset). Fits for two main features that are symmetric around V_{sys} are overlaid, together with two narrower "suggestive" features that are also symmetric but otherwise similar to the noise peaks even after stronger smoothing.

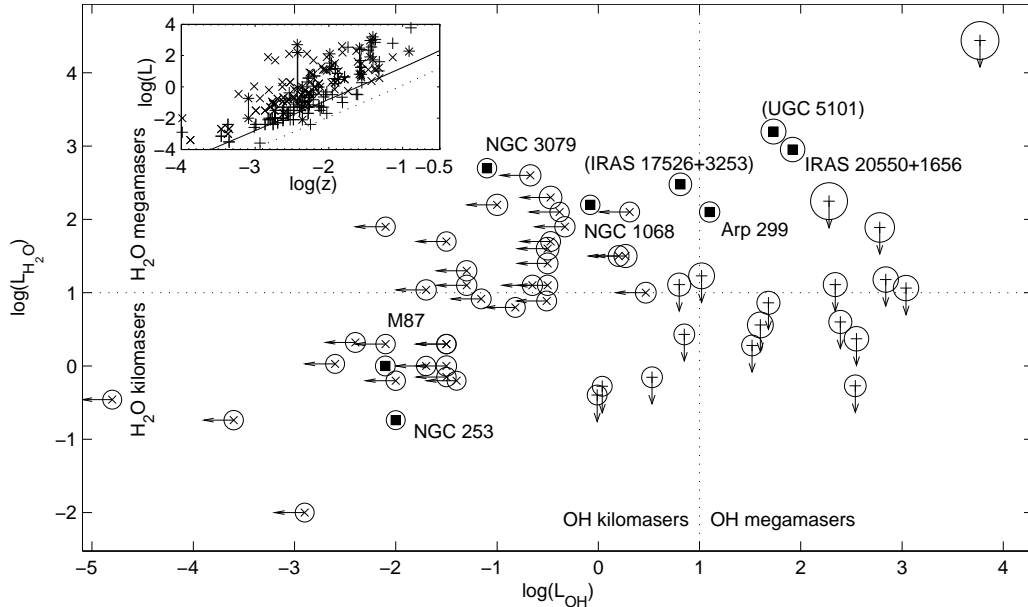


Fig. 2. Equivalent isotropic luminosities and 3σ upper limits (arrows) for 61 sources detected in one or both of the 1.6 GHz OH and 22 GHz H_2O maser species, with 35 detected in H_2O only (x) and 18 in OH only (+). The circle diameters are proportional to the source redshift. The OH MM sources tend to have a higher redshift. Masers of both species may be found in up to 8 sources (solid squares; source names given), with the caveat that the OH KM in UGC 5101 and IRAS 17526+3253 reported by Martin et al. (1989) were not detected in later (or earlier) observations. The inset shows OH and H_2O luminosities or 3σ upper limits against redshift for the 61 detected sources and for 34 sources undetected in either species. The H_2O and OH detection thresholds (solid and dashed lines) assume 1.0 mJy rms and a 2.0 km s^{-1} FWHM.